European Journal of Pharmaceutics and Biopharmaceutics 142 (2019) 435–448

Contents lists available at ScienceDirect

European Journal of Pharmaceutics and Biopharmaceutics

journal homepage: www.elsevier.com/locate/ejpb

Research paper

Bridging *in vitro* dissolution and *in vivo* exposure for acalabrutinib. Part II. A mechanistic PBPK model for IR formulation comparison, proton pump inhibitor drug interactions, and administration with acidic juices

Xavier J.H. Pepin[a,*], Andrea J. Moir[a], James C. Mann[a], Natalie J. Sanderson[a], Richard Barker[a], Elizabeth Meehan[a], Allan P. Plumb[a], George R. Bailey[a], Dean S. Murphy[a], Cecile M. Krejsa[b], Marilee A. Andrew[b], Timothy G. Ingallinera[b], J. Greg Slatter[b]

[a] *AstraZeneca, Pharmaceutical Technology and Development, Charter Way, Macclesfield SK10 2NA, United Kingdom*
[b] *Acerta Pharma, 121 Oyster Point Blvd, South San Francisco CA 94080, USA*[1]

ARTICLE INFO

Keywords:
PBPK modelling
Dissolution
In vitro-in vivo correlation
Mechanistic
Fruit juice
Proton pump inhibitor
Particle size distribution

ABSTRACT

Acalabrutinib (Calquence®) 100 mg (bid) has received accelerated approval by FDA for the treatment of adult patients with mantle cell lymphoma (MCL) who have received at least one prior therapy. Acalabrutinib is a substrate of PgP and CYP3A4, with a significant fraction of drug metabolized by first pass gut extraction and 25% absolute bioavailability. The absorption of acalabrutinib is affected by stomach pH, with lower pharmacokinetic exposure observed following co-administration with proton pump inhibitors.

During dissolution at pH values below its highest basic pKa, the two basic moieties of acalabrutinib react with protons from the aqueous solution, leading to a higher pH at the drug surface than in the bulk solution. A batch-specific product particle size distribution (P-PSD), was derived from dissolution data using a mechanistic model that was based on the understanding of surface pH and the contribution of micelles to the dissolution rate. P-PSD values obtained for various batches of acalabrutinib products in simple buffers, or in complex fluids such as fruit juices, were successfully integrated into a physiologically based pharmacokinetic (PBPK) model developed using GastroPlus v9.0™. The integrated model allowed the prediction of clinical pharmacokinetics under normal physiological stomach pH conditions as well as following treatment with proton pump inhibitors. The model also accounted for lower pharmacokinetic exposure that was observed when acalabrutinib was co-administered with the acidic beverages, grapefruit juice, (which contains CYP3A inhibitors), and orange drink (which does not contain CYP3A inhibitors), relative to administration with water.

The integration of dissolution data in the PBPK model enables mechanistic understanding and the establishment of more robust *in vitro-in vivo* correlations (IVIVC) under a variety of conditions. The model can then distinguish the interplay between dissolution and first pass extraction and how *in vivo* stomach pH, saturation of gut PgP, and saturation or inhibition of gut CYP3A4, will impact the pharmacokinetics of acalabrutinib.

1. Introduction

Bridging *in vitro* dissolution and *in vivo* absorption has been of interest to regulators, academics and the pharmaceutical industry for many years [1–3]. The establishment of valid Level A *in vitro-in vivo* correlations (IVIVC) allows waiving certain clinical trials and a stronger positioning of Quality by Design spaces [4]. There are still hurdles in developing these correlations since the percentage of regulatory submissions containing IVIVCs is only around 30% [5]. Classical IVIVCs are mathematical relationships between *in vivo* absorption rate and *in vitro* dissolution and this limits their applicability to certain scenarios. IVIVC typically cannot be used to predict clinical outcomes across different doses when there is an *in vivo* solubility limitation, different administration conditions, different species or varying physiological conditions.

Finding dissolution conditions that perfectly match the *in vivo* absorption rates for different formulations may be complicated by the fact that *in vivo* absorption can be limited by factors other than dissolution, such as transit or permeability, and by the fact that *in vivo* dissolution is

* Corresponding author.
E-mail address: xavier.pepin@astrazeneca.com (X.J.H. Pepin).
[1] At the time of manuscript preparation.

https://doi.org/10.1016/j.ejpb.2019.07.011
Received 22 March 2019; Received in revised form 20 June 2019; Accepted 11 July 2019
Available online 12 July 2019
0939-6411/

happening in an ever-changing environment. Okumu et al. relied on dynamic dissolution methods to establish IVIVC [6] but these are rarely used in routine QC release testing. There could also be dissolution differences that do not result in *in vivo* exposure differences, as illustrated in the concept of safe space [7]. This precludes the establishment of a classical IVIVC.

For all of these reasons, alternative methods to derive IVIVCs have emerged based on the use of physiologically based pharmacokinetic (PBPK) model platforms, in which the gastro-intestinal tract is described as a series of compartments, with volumes, pH, transit times, and surfaces that mimic the physiological reality. In these models, the absorption rate is mechanistic, i.e. specifies the simultaneous or sequential events leading to absorption, including dissolution, precipitation, permeation and transit. In addition, factors such as first pass gut extraction and active influx or efflux are incorporated to the different gastro-intestinal compartments of these models, and can modulate the amount of drug reaching the portal vein. These IVIVCs are usually termed “mechanistic” or “PBPK based” [2] and grouped under the umbrella of Physiological Based Biopharmaceutics Modelling (PBBM) [3]. They represent an interesting alternative to classical IVIVCs, since they can incorporate the impact of physiological variables on dissolution and absorption.

The best way to integrate drug product dissolution data with PBPK tools is a matter of debate [8,9], and some approaches may be more appropriate for certain formulation types or certain drug properties. The use of mathematical models, such as Weibull functions, to fit observed dissolution profiles, can provide clinically relevant inputs for immediate release or modified release formulations of Biopharmaceutics Classification System (BCS) class 1 drugs, for which the *in vitro* and *in vivo* dissolution is expected not to depend on volume or pH [10]. However, when the drug is an immediate release formulation and when dissolution depends on medium pH and drug substance particle size, the use of a more mechanistic model such as the Noyes-Whitney equation to analyze dissolution and integrate it into the PBPK model is recommended. Recently a Product Particle Size Distribution (P-PSD) based on this approach was proposed for formulations containing lesinurad, a weak acid, as the most clinically relevant method to integrate dissolution in PBPK models [8].

For weakly basic drug substances, the impact of different stomach pH values on the predicted human exposure is usually evaluated both pre-clinically and clinically and modelled *a priori* using PBPK tools and sensitivity analysis. If the formulation or the active ingredient is sensitive to pH, the between-subject and within-subject variability of gastro-intestinal (GI) tract pH are important factors to integrate in PBPK simulations when assessing the equivalence of drug formulations [11,12].

Natural variation in human stomach pH occurs throughout the day [13,14] and following food ingestion [15]. Many patients are treated with acid reducing agents (ARAs) or show altered stomach pH due to race and/or age [16,17]. Diseases such as H. Pylori infections or gastric cancer can also alter acid secretion in the stomach [18,19]. For some drugs, stomach pH and gastric emptying time variations may limit the extent of drug dissolution prior to absorption and may lead to variability in pharmacokinetic (PK) exposure as assessed by C_{max} and/or AUC. Recent papers point out issues associated with drug interactions between oral targeted anticancer agents and proton pump inhibitors [20,21], which can be overcome in certain cases by administration of the drug with acidic beverages [22].

Most commercial *in silico* PBPK software platforms, including GastroPlus™, lack certain key aspects of the dissolution process, even when mechanistic dissolution is used. Current concerns are the consideration of how bulk drug solubility drives the dissolution rate calculation, the application of the same unstirred water layer (UWL) thickness for both free drug and drug bound to micelles, and the lack of impact of reactive media constituents on the dissolution rate calculation. As discussed in Pepin et al. [45], for substrates which react with dissolution medium components, the diffusion and reaction rates of all species in the UWL should be considered in the calculation of dissolution rate [23,24].

For a weak base, the influence of surface pH on surface solubility can be important below the maximum basic pKa, and this should be considered in some, or all of the GI-tract compartments in PBPK models, depending on the drug pKa. For acalabrutinib (maximum basic pKa of 5.77), only the stomach compartment is impacted by differences between surface pH and bulk pH. To remediate this PBPK platform deficiency in surface pH calculation, Cristofoletti et al. manually altered the stomach pH in the physiological compartmental model to represent surface pH in the dissolution rate calculation [11]. We have used the same approach in this work and proposed theoretical equations to predict surface pH from drug properties in non-buffered conditions typical of the gastric environment. These equations could be implemented as permanent features in PBPK models to calculate relevant dissolution rates from surface pH for reactive substances [45].

The PBPK model strategy followed in this work consisted of 4 steps. The model set-up, which was a top-down analysis of an absolute bioavailability study where 8 subjects were dosed with 100 mg acalabrutinib capsules and an intravenous microdose at oral dose t_{max}. Following the model set-up, a sensitivity analysis was conducted to see which parameters are most influential on acalabrutinib pharmacokinetics. The model verification and validation consisted of checking whether the 8-subject population in the PBPK model could reproduce clinical observations obtained in 16 different scenarios from 5 independent clinical studies. Finally, the model use consisted of determining the safe space for drug substance particle size.

2. Materials & methods

2.1. Biopharmaceutical properties of acalabrutinib

Acalabrutinib is a BCS class II drug with biopharmaceutical properties: MW 465.5 g mol^{-1}, true density = 1.34 g mL^{-1}, fraction unbound in plasma $f_{u,p}$ = 2.6%, blood to plasma ratio = 0.787, pKa values = 3.54 (base), 5.77 (base) and 12.1 (acid), intrinsic solubility = 48 µg/mL at pH 8, log P = 2.0. The measured aqueous pH solubility profile matches the theoretical profile, given by the ionization constants and intrinsic solubility at pH 8. The solubility in Fasted State Simulated Intestinal Fluid (FaSSIF v2) [25], and Fed State Simulated Intestinal Fluid (FeSSIF) [26] were 0.12 mg/mL and 0.67 mg/mL respectively. Solubility in simulated intestinal media allowed calculation of the drug solubilization ratio, using the in-built calculation tool of the PBPK model. The effect of micelles was also considered for the calculation of the *in vivo* dissolution in the software. The absolute bioavailability of a 100 mg acalabrutinib capsule is around 25%, with anticipated complete absorption. Approximately 50% drug is metabolized by CYP3A4 first pass gut extraction and 50% drug metabolized by first pass liver extraction (study ACE-HV-009). The percentage of total fecal excreted dose recovered as unchanged drug in the feces was 1.2%, which suggests complete absorption. There was no drug degradation *in vitro* over the physiological pH range. The drug precipitation was ignored in the model based on *in vitro* and *in vivo* evidence presented in the supplementary materials.

2.2. Materials

Simulated gastric fluid pH 1.2 and pH 1.8 (SGF) were prepared using concentrated HCl (Sigma Aldrich) and sodium chloride (Sigma Aldrich). Double concentrated fasted state simulated intestinal fluid, version 2, (2X FaSSIF-V2) [25] was prepared using sodium taurocholate hydrate (Sigma Aldrich), lecithin (Lipoid), sodium hydroxide (Sigma Aldrich), sodium phosphate (Sigma Aldrich) and sodium chloride (Sigma Aldrich). Note that the buffer from FaSSIF-V1 [26] was used for analytical reasons (phosphate instead of maleate as buffer salt) but with

FaSSIF-V2 bile salt and lecithin levels. Capri-Sun™ orange drink (Kraft Foods) used in the dissolution studies was sourced locally in the US. Grapefruit juice (Sainsbury's) used in the dissolution studies was sourced locally in the UK.

Five clinical batches of acalabrutinib capsules studied were: 2.5 mg phase 1 capsule (batch NCZP), 25 mg phase 1 capsule (batch NCZS), 100 mg capsule phase 1 formulation (batch NVTF), two commercial representative formulations of 100 mg capsule (batch L0505009 and batch W026394). Acalabrutinib drug substances and reference standard were sourced internally.

2.3. Permeability

Acalabrutinib apparent permeability (P_{app}) was measured in bidirectional Transwell™ assay, using MDCK-MDR1 cells cultured in 96 well plates. Each well had a filter surface area of 0.11 cm^2 and a cellularity of 45,000 cells per well. All buffers used in the experiments consisted of Hanks' Balanced Salt Solution (HBSS) (Invitrogen, Lidingö, Sweden) containing 25 mmol/L N-2-hydroxyethyl-piperazine-N-2-ethanesulfonic acid (HEPES) (Invitrogen, Lidingö, Sweden) adjusted to pH 7.4 (HBSS-HEPES, pH 7.4). The apical buffer volume was 150 µL, and the basolateral volume was 300 µL. Permeability was measured in both directions using drug concentrations of 1, 5, 10, 30, 50, 75, 100, 150, 200 µM. The measurements were done in triplicate. Data for amount drug permeated was gathered at 15, 45, 90 and 120 min and the apparent permeability calculated after 2 h equilibration according to the following equation:

$$P_{app} = \frac{dQ}{dt} \times \frac{10^6}{A \times C_D}$$

where dQ/dt is the slope of amount permeated versus time, A is the filter area and C_D the drug concentration in the donor compartment. The kinetic parameters V_{max} and K_m for PgP were determined for acalabrutinib using the method of Tachibana et al. [27], with simultaneous fitting of apical to basal and basal to apical permeability values. The Tachibana equations calculate K_m relative to the intracellular unbound drug concentration as a function of drug donor concentration, passive permeability and active efflux. This treatment of permeability data provides more consistent determinations of K_m values, even when obtained from different cell lines. The PgP functionality of the MDCK-MDR1 cells used for acalabrutinib testing, was assessed by measuring the apparent permeability values of digoxin: $P_{app,A2B} = 1.6 \pm 0.4 \cdot 10^{-6}$ cm/s and $P_{app,B2A} = 36.6 \pm 1.85 \cdot 10^{-6}$ cm/s. These values are not significantly different from the ones reported for digoxin by Troutman and Thakker [28] ($P_{app,A2B} = 1.89 \pm 0.13 \cdot 10^{-6}$ cm/s and $P_{app,B2A} = 35.7 \pm 1 \cdot 10^{-6}$ cm/s), which indicate similar PgP functionality in both systems. MDCK-MDR1 cells express PgP to approximately the same level relative to the duodenum [28]. In the chosen PBPK model, the reference PgP expression is taken for the colon for which there is a 2-fold higher expression level compared to the duodenum. Therefore, V_{max} values determined from MDCK-MDR1 cells *in vitro* were multiplied by a factor of 2 prior to entry into the PBPK model unit converter. The apparent passive permeability from *in vitro* MDCK-MDR1(extracted from the Tachibana data analysis) was scaled to human effective jejunal permeability using cyclosporin, ranitidine and verapamil apparent permeability values measured by Troutman and Thakker [28] and the effective human jejunal permeability values measured by Lennernäs [29].

2.4. Powder surface area

Acalabrutinib (approximately 1 g) was degassed under vacuum at 30 °C for a minimum of 14 h. The nitrogen sorption isotherm was determined from 0.01 to 0.95 P/P_0 using a Tristar 3000 surface area analyzer (Micromeritics). The Specific Surface Area (SSA) was determined by the method of Brunauer, Emmett and Teller (BET) from sorption data collected between 0.05 and 0.30 P/P_0.

2.5. Drug substance SEM images

Acalabrutinib particles were imaged by scanning electron microscopy (SEM) using a Hitachi TM-1000 microscope at an accelerating voltage of 15 kV. Samples were mounted on an aluminum stub using a double-sided adhesive carbon conductive tape and gold sputter coated 10 nm for 3 min. Images were taken at set magnifications (×50, ×100, ×250, ×500 and ×1000) so that direct comparisons between the samples could be made.

2.6. Particle size distribution by laser diffraction

Particle size distribution was measured by laser diffraction using a Mastersizer 3000 and equipped with an Aero S sample dispersion unit (Malvern) and using the Fraunhofer optical model. The dispersion pressure was set to 2 bars and the sample amount for each determination was 500 mg. The instrument software was used to calculate $D_{(v,0.1)}$, $D_{(v,0.5)}$ and $D_{(v,0.9)}$ for the particle size distribution which are the particle diameters corresponding to 10%, 50% and 90% of the cumulative undersize distribution (by volume).

2.7. Surface pH

The surface pH of acalabrutinib slurries was measured in unbuffered HCl solutions of different molarities and phosphate buffer at pH 6.8 using the technique of Serajuddin et al. [30]. The results and theoretical equations presented in detail in the companion paper [45]. The full bulk pH solubility profile for acalabrutinib is entered in the PBPK platform, however the stomach pH was adjusted to that of acalabrutinib surface pH, based on previous approaches in different PBPK platforms [11]. Using the theoretical equation for acalabrutinib, the normal default value for fasted bulk stomach pH in the PBPK model is increased from 1.3 to 3.55 to account for surface pH. For modelling ARA treatment, the stomach pH in the PBPK model is increased to pH 5.54, which corresponds to the surface pH of acalabrutinib crystals when the bulk pH is at 5. This pH is that of the dosing water, assuming it controls the pH of stomach where hydrochloric acid secretion is inhibited.

2.8. Mechanistic evaluation of in vitro drug product dissolution

To integrate *in vitro* dissolution data from clinical batches in the PBPK model, a mechanistic approach was used. Pepin et al. [8] have reported several methods to integrate *in vitro* dissolution data in PBPK platforms. The use of tabulated dissolution vs time data or Weibull function fitting of dissolution data was ruled out for acalabrutinib, since these approaches would not allow prediction of the impact of stomach pH by changing the physiological parameters of the PBPK model. The use of the Z-factor [31] was also ruled out, since it did not allow adequate fitting of the *in vitro* dissolution data over the entire release time. Instead, we have used a Product Particle Size Distribution (P-PSD), which is calculated from *in vitro* product batch dissolution data. For each batch of acalabrutinib capsules, a single P-PSD could explain all the *in vitro* dissolution conditions tested, in simple and complex media throughout the physiological pH range and in the presence of natural or synthetic surfactants. Detailed analysis of the *in vitro* dissolution profiles and associated equations are presented in Pepin et al. [45]. For early clinical batches, the QC method was used to extract drug product P-PSD. For later batches, dissolution in phosphate pH 6.8 was used to extract P-PSD.

In addition to product dissolution in simple buffers and biorelevant media at 37 °C, the dissolution of 100 mg acalabrutinib capsule batch L0505009 was also assessed in 240 mL water, grapefruit juice or orange drink at room temperature after addition to 60 mL pH 1.2 simulated gastric fluid (SGF) preheated in a bath at 37 °C (Fig. 3). After 30 min,

300 mL of a preheated double concentrated, fasted state simulated fluid (2X FaSSIF-V2) medium were added to shift the conditions to a final intestinal pH of 6.5 and FaSSIF-V2 composition. A USP apparatus 2 (Distek 2100) was used at 50 rpm with sampling in the SGF-beverage phase at 10, 20, 30 min and sampling in the FaSSIF-V2 phase at 45, 60, 90 and 120 min. Samples were filtered immediately using 1 µm 25 mm glass fiber syringe filters (PALL) with 3 mL discarded to waste. Samples were then stabilized by immediately diluting the filtrate 1:1 with acetonitrile. Dissolution samples were analyzed against an external reference standard using an HPLC-UV method on an Agilent 1100 fitted with a VWD UV detector. Mobile phases of 10 mM ammonium acetate and acetonitrile were used with gradient elution on a Phenomenex Ultracarb ODS, column (100 mm × 4.6 mm, 5 µm). The injection volume was 10 µL and detection wavelength was 285 nm. A P-PSD was also extracted for dissolution of batch L0505009 in juices.

2.9. Clinical study summary

Clinical pharmacokinetic data used in the PBPK model development and validation were from studies ACE-HV-001, ACE-HV-004, ACE-HV-005, and ACE-HV-112 (Celerion, Tempe, Arizona, USA), ACE-HV-112 (Celerion, Lincoln, Nebraska, USA), and ACE-HV-009 (Covance, Madison, Wisconsin, USA). All studies were carried out in accordance with the US Code of Federal Regulations, GCP, 21 CFR Parts 50, 56, and 312, the ethical principles set forth in the Declaration of Helsinki, and the ICH harmonized tripartite guideline regarding GCP (E6 Consolidated Guidance, April 1996) and the ethical requirements referred to in the European Union (EU) directive 2001/20/EC. The summary of clinical design and main results for the clinical studies are presented in supplementary Table S1.

2.10. PBPK modelling strategy

The PBPK modelling strategy is summarized in Fig. 1. The model was built using PK data from a micro-dose human absolute bioavailability study (ACE-HV-009), verified and validated with PK data from studies ACE-HV-001 [32], ACE-HV-004, ACE-HV-005 [33], ACE-HV-112 and ACE-HV-113. The model verification and validation consisted of checking the ability of the model developed on the population of ACE-HV-009, to reproduce 16 clinical outcomes of 5 independent clinical studies by changing relevant model physiological parameters (stomach pH and inhibition of gut CYP3A4) and drug product batch P-PSD. For model verification and validation, the population parameters resulting from model set up were kept the same, and no measures were taken to adapt population co-variates or individual drug distribution and disposition parameters to other clinical scenarios. Finally, the model was used to predict the safe space for acalabrutinib drug substance particle size distribution.

2.10.1. PBPK model set-up

The model was set up using data from absolute bioavailability study ACE-HV-009 cohort 1 (Table 2). Individual PK data were used to create a population of 8 subjects for which both intravenous and oral plasma data were available. Total clearance, volume of distribution and 3 compartment distribution micro-constants were extracted from the eight individual IV profiles. The contribution of renal clearance was neglected, since measured renal clearance of acalabrutinib represents 3 percent of the total clearance. For oral data, the individual hepatic first pass extractions were calculated with the well stirred model, assuming that total intra-venous clearance was metabolic, and using the average acalabrutinib blood to plasma ratio measured *in vitro*. In the PBPK model, the percent default values for volume occupation by water in the small intestine and colon (40% and 10% respectively), were reduced to 7.5% and 2% respectively, to better account for measured free water content in the small intestine and colon [8,34]. A gastric retention time was added for each subject to match observed lag times in the pharmacokinetic profiles and improve modelling accuracy (see supplementary material). All the parameters used in the PBPK model building, based on observed individual PK and *in vitro* data, are given in Table 1.

Table 1 shows that the only drug related parameter fitted to the individual oral profiles is the gut CYP3A4 V_{max}. This parameter will modulate the extent of drug reaching the portal vein and can be fitted to oral absorption profiles separately from the systemic disposition parameters which are derived from individual intra-venous PK data. Lown et al. [35] have reported variability in gut CYP3A4 expression. Depending on the marker used for CYP3A4 expression, inter-subject variability is high, at 11-fold based on protein content, 8-fold based on mRNA and 6-fold based on catalytic activity (1′-OH midazolam formation). This heterogeneity in stomach transit time and gut V_{max} were considered in model building and are also reported in the sensitivity analysis.

2.10.2. Sensitivity analysis

Using subject S013 of ACE-HV-009 as a representative subject from the ACE-HV-009 study population (based on total clearance, volume of distribution and gut CYP3A4 V_{max}), several physiological and drug related parameters were varied to assess the parameters exerting the most influence on PK. The parameters varied during the sensitivity analysis are reported in Table 2. C_{max} and AUC_{0-t} were calculated and represented versus the baseline simulation and 0.8–1.25 fold interval around the baseline simulation.

2.10.3. Model verification and validation

Model validation assessed the ability of the ACE-HV-009 eight subject population to provide adequate mean values for AUC_{0-t} and C_{max} for different clinical populations, with different formulations and/or dose or administration schemes. The systemic clearance and gut first pass extraction of acalabrutinib are correlated and systemic clearance is a function of subject co-variates. Running virtual trials in the PBPK model was therefore ruled out since the software applies random variation in clearance and V_{max} without considering their link to population co-variates. Predictions from the same population from ACE-HV-009 were used without adjusting the system parameters, to test how representative that population was of different clinical trial populations. Parameters that were varied in the model validation and those which were kept constant are reproduced in Table 3 for each clinical scenario tested in the validation. This table shows that the only inputs which were varied to reproduce the clinical scenarios, were the drug product batch P-PSD, the stomach pH, to account for dosing the drug with and without omeprazole pre-treatment, and the scaling factor of gut CYP3A4 V_{max}. This last parameter was set to 0.3 for all individuals when applicable, to reflect the time inhibition of gut CYP3A4 by grapefruit juice [36].

Out of the 16 clinical scenarios simulated, 15 had measured pharmacokinetic parameters reported in the clinic. An additional scenario was simulated to assess the impact of grapefruit juice time dependent inhibition of gut CYP3A4, i.e. pre-treatment with grapefruit juice and drug administration with water.

To assess model performance, the average fold error (AFE) and absolute average fold error (AAFE), were calculated for the prediction of AUC_{0-t} and C_{max} across the 16 clinical scenarios tested. The average fold error indicates whether the predicted values underestimate or overestimate the observed values. The absolute average fold error quantifies the absolute error from the true value.

$$AFE = 10^{\frac{1}{n}\times\sum \mathrm{Log}\left(\frac{\mathrm{predicted_i}}{\mathrm{observed_i}}\right)}$$

$$AAFE = 10^{\frac{1}{n}\times\sum \left|\mathrm{Log}\left(\frac{\mathrm{predicted_i}}{\mathrm{observed_i}}\right)\right|}$$

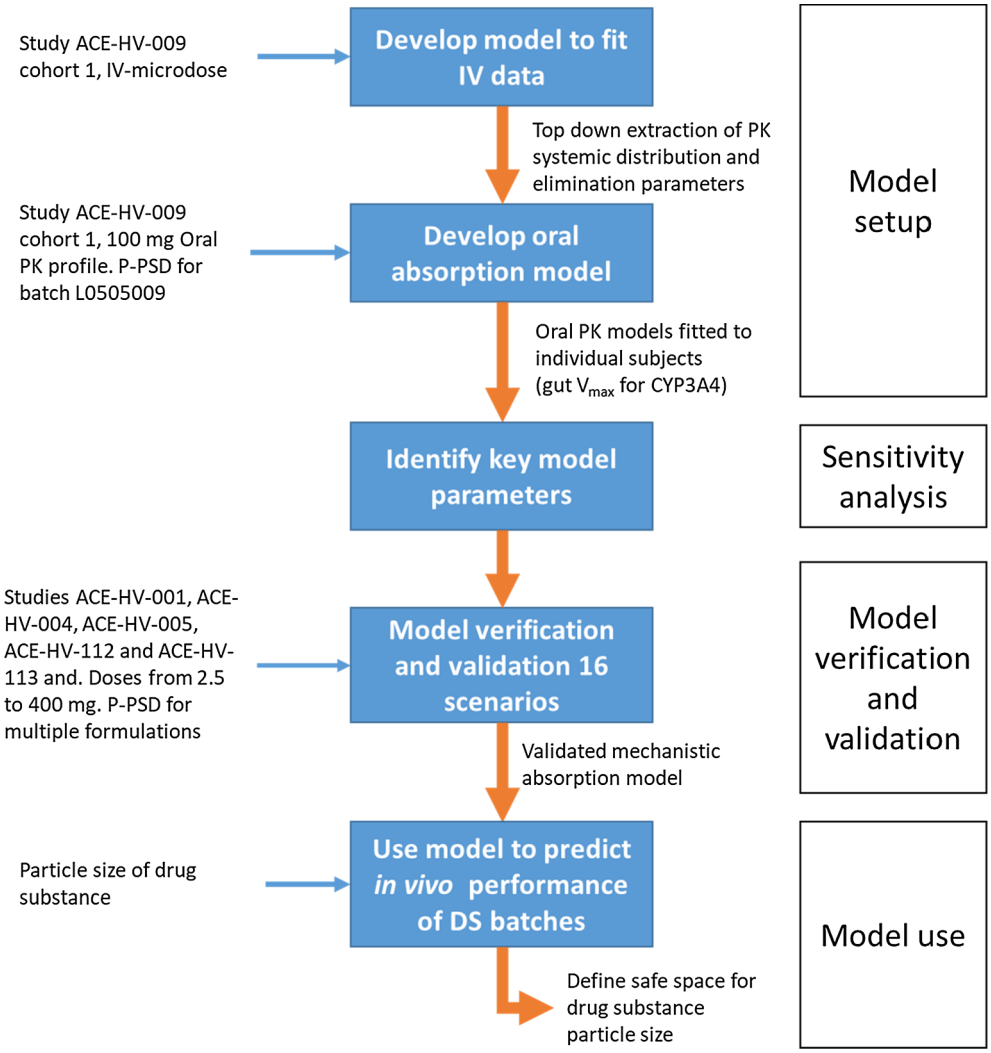

Fig. 1. PBPK Modelling strategy for acalabrutinib.

3. Results and discussion

3.1. Permeability of acalabrutinib

Fig. 2 shows the evolution of apical to basal and basal to apical apparent permeability for acalabrutinib in MDCK-MDR1 versus concentration, and the fit obtained with the Tachibana model. The model parameters were $V_{max} = 79.6 \cdot 10^{-6}\,\mu g\,s^{-1}$, $K_m = 5.97\,\mu M$ and passive permeability $= 15.2 \cdot 10^{-6}\,cm\,s^{-1}$.

Using the correlation to human P_{eff}, the effective human jejunal permeability for acalabrutinib was estimated at $5.4 \cdot 10^{-4}\,cm\,s^{-1}$.

3.2. Dissolution of drug products and P-PSD

The 100 mg acalabrutinib capsule batch L0505009 dissolution rate in room temperature orange drink, grapefruit juice and water are shown in Fig. 3.

The drug dissolution in juices was similar and approximately 3-fold slower than dissolution in room temperature water, despite a similar surface pH and surface solubility of the drug. The surface pH of acalabrutinib was 3.8 in SGF and orange drink, 3.6 in SGF and grapefruit juice, and 3.9 in SGF and water. The slower dissolution rate of acalabrutinib in juices was in part attributed to dissolution at room temperature (which could play on solubility and viscosity) and to the presence of weak organic acids in the juice which could react with acalabrutinib and slow down dissolution (see supplementary Table S3). Since the model used does not account for the diffusion of reactive species in the calculation of drug dissolution, a new P-PSD for dissolution of batch L0505009 in juices was fitted using the surface pH measured in the juices and the average profile for orange drink and grapefruit juice. Following pH shift to the FaSSIF-V2 medium, the dissolution of acalabrutinib is essentially halted since it becomes solubility limited.

Dissolution of other clinical batches in simple media and fitting of all dissolution experiments are shown in the supplementary materials and P-PSDs extracted from fitting the dissolution data are presented in Fig. 4.

3.3. PBPK model set-up

Study ACE-HV-009 cohort 1, comprised five male and three female healthy human volunteers aged from 30 to 62 years old. No difference in disposition parameters was observed based on sex. Individual ADME parameters obtained for the eight subjects in ACE-HV-009 are shown in Table 4. The only parameter that was individually fitted to the oral profiles in the model was the V_{max} for gut CYP3A4. As previously explained, inter-subject variability for gut CYP3A4 V_{max} is expected to range from 6 to 11-fold. The observed variability of the fitted gut CYP3A4 V_{max} is 12-fold, which is in accordance with literature values.

The fits of IV and oral plasma data are presented in supplementary

Table 1
Drug related parameters for the PBPK model.

Parameter (unit)	Selected value	Justification
Molecular weight ($g\,mol^{-1}$)	465.5	From structure
pKa values in physiological range	3.54 (base) and 5.77 (base)	Measured *in vitro*
Log P	2.0	Measured
Diffusion coefficient 10^{-9} cm/s	0.6069	Calculated by model based on density and molecular weight
True density (g/mL)	1.34	Measured
Intrinsic solubility @ pH 8 (μg/mL)	48	Measured
Aqueous solubility vs pH	Calculated from intrinsic solubility data	Calculated by model and in accordance with measured data
FaSSIF-V2 solubility (mg/mL)	0.12	Measured
FeSSIF solubility (mg/mL)	0.67	Measured
Precipitation time (s)	100,000	See supplementary material
Fraction unbound in plasma (%)	2.6	Measured *in vitro* in human plasma
Blood to plasma ratio	0.87	Measured *in vivo* in human blood
Effective permeability 10^{-4} cm/s	5.4	Constant from MDCK-MDR1 data (see Section 3.1)
Bile salt effect for dissolution	ON	NA
Solubilization ratio (no unit)	1.2E4	Calculated by model based on FaSSIF-V2 & FeSSIF solubility data
The diffusion coefficient is adjusted for bile salt effect	ON	Default model option
Dissolution model	Johnson model with a maximum diffusion layer thickness of 30 μm	Default model mechanistic dissolution model
Gut V_{max} CYP3A4 ($mg\,s^{-1}$)	Variable	Fitted to individual oral profiles from ACE-HV-009
Gut K_m CYP3A4 (mg/L)	20	Constant fitted to oral profiles from ACE-HV-009
Drug substance particle size	P-PSD extracted from *in vitro* product dissolution data	See Section 3.2
Gut V_{max} P-gp (mg/s)	4.22E-03	Constant and extracted from *in vitro* data from MDCK-MDR1 cells (see Section 3.1)
Gut K_m P-gp (mg/L)	2.78	Constant and extracted from *in vitro* data from MDCK-MDR1 cells (see Section 3.1)

Table 2
Sensitivity analysis for acalabrutinib exploring physiological and drug related parameters.

Param Name	Lower Limit	Baseline	Upper Limit
P_{eff} (10–4 cm/s)	2.7	5.4	10.8
Solubility (mg/mL)	0.0048	0.048	0.48
Volume of fluid Small Intestine (%)	3.75	7.5	15
Stomach transit time (h)	0.125	0.25	0.5
Stomach pH	0.5	3.55	8
Efflux K_m scaling factor	0.5	1	2
Efflux V_{max} scaling factor	0.5	1	2
Gut K_m scaling factor	0.5	1	2
Gut V_{max} scaling factor	0.5	1	2

material. From the individual PK profile analysis, the clearance and V_{SS} that can be calculated from Table 4 data show more than 2 and 8-fold variability, respectively without a clear link to body weight. This suggests that in the absence of intravenous data to measure these parameters, the prediction error of a PBPK model using clearance and distribution volume normalized by body weight would be important, and confirms that the approach for individual modelling based on IV data is appropriate for this compound [37].

3.4. Sensitivity analysis

The Parameter Sensitivity Analysis (PSA) data for S013 receiving a 100 mg dose are presented for C_{max} and AUC_{0-t} in Figs. 5 and 6 respectively. The grey horizontal dashed line represents the baseline prediction and the grey horizontal solid lines represent the 0.8 to 1.25-fold interval around the baseline prediction.

Sensitivity analysis shows that acalabrutinib intrinsic solubility does not have a major influence on acalabrutinib bioavailability. A reduction of 10-fold in intrinsic solubility at pH 7 does not lead to a major reduction in bioavailability (about 40% reduction in C_{max} and AUC). Since acalabrutinib is a diprotic base, solubility in acidic conditions is high enough to ensure complete dissolution of the 100 mg dose, even with reduced intrinsic solubility. Furthermore, the absence of precipitation upon gastric emptying increases the safety margin for the impact of a reduced intrinsic solubility.

In addition, V_{max} and K_m for efflux transporters are not anticipated to impact exposure within the ranges tested in Table 2. With the 100 mg dose, efflux transporters are saturated, and therefore the impact of changing the scaling factor for efflux transporters on predicted exposure is limited.

The volume of liquid in the small intestine and gut CYP3A4 K_m scaling factors are anticipated to lead to variations in C_{max} and AUC within the 0.8–1.25 fold range of baseline. Stomach transit time has a stronger effect on C_{max} than AUC as expected and the negative correlation of AUC and stomach transit time can be attributed to larger first pass extraction due to dilution. In reality, acalabrutinib capsules dissolve in the stomach and are retained until the stomach content is rapidly released, leading to observable lag-times in the individual PK profiles. The drug permeability, gut CYP3A4 V_{max} scaling factor, and pH are expected to lead to the largest variations in C_{max} and AUC. Since on average, approximately 50% of the dose is metabolized by first pass gut extraction, the impact of changes in CYP3A4 expression or activity in the gut is significant. Similarly, pH is anticipated to have strong impact on acalabrutinib exposure. A pH increase from acidic to neutral is anticipated to reduce C_{max} by 10-fold and AUC by 2-fold.

The system parameters that are most influential are stomach pH on C_{max} and AUC_{0-t}, and stomach transit time on C_{max}. The drug parameters that are most influential are permeability and gut CYP3A4 V_{max} scaling factors on both C_{max} and AUC_{0-t}. In a cross-over trial with a wash-out period, the 2 latter parameters are expected to be constant. The sensitivity of C_{max} and AUC to acalabrutinib permeability is explained by the large amount of drug metabolized by first pass gut extraction (50% on average). Even if the extent of absorption does not vary significantly for a 100 mg dose in the effective permeability range tested, the rate at which the drug crosses the gut membrane will contribute to determine the extent of first pass extraction for a given subject. For subject S013, varying the P_{eff} from 2.7 to $10.8 \cdot 10^{-4}$ cm s^{-1} does not significantly alter the fraction absorbed which goes from 94% to 99.8% but significantly reduces the gut first pass extraction from 76% to 45%.

To understand variability in clinical PK data, important parameters to measure are the stomach pH, acalabrutinib permeability, gastric

Table 3
Parameters used for PBPK model validation for 16 clinical scenarios tested.

Clinical scenario tested	Parameters				
	Dose administered	Vc, distribution micro-constants, CL_T, body weight, effective permeability, stomach residence time, stomach gastric emptying post residence time, gut V_{max} and K_m for PgP, gut K_m for CYP3A4	Gut V_{max} for CYP3A4	In vitro dissolution (P-PSD)	Stomach pH
ACE-HV-001 Normal stomach pH + batches NCZP or NCZS with water	2.5, 5, 25, 50, 75 and 100 mg	No change compared to ACE-HV-009	No change compared to ACE-HV-009	Batch NCZP or NCZS from observed *in vitro* dissolution data in HCl 0.1 N	3.55(B)
ACE-HV-113 Normal stomach pH + batch W026394 with water	100 mg			Batch W026394 from observed *in vitro* dissolution data in simple buffers)	
ACE-HV-004 Normal stomach pH + batch NVTF with water	100 mg			Batch NVTF from observed *in vitro* dissolution data in HCl0.1 N	
ACE-HV-004 Omeprazole pre-treatment + Batch NVTF with water	100 mg			Batch L0505009 from observed *in vitro* dissolution data in simple buffers	5.54(C)
ACE-HV-005 Normal stomach pH + batch L0505009 with water	100 mg and 400 mg				3.55(B)
ACE-HV-112 Normal stomach pH + batch L0505009 with water	100 mg				
ACE-HV-112 Omeprazole pre-treatment + batch L0505009 with water	100 mg				5.54(C)
ACE-HV-112 Normal stomach pH + batch L0505009 with orange drink	100 mg			Batch L0505009 from observed *in vitro* dissolution data in juices	3.8(D)
ACE-HV-112 Normal stomach pH + batch L0505009 with grapefruit juice after grapefruit juice pre-treatment	100 mg		Individual V_{max} from ACE-HV-009 with scaling factor of 0.3(A)		
ACE-HV-112 Normal stomach pH + batch L0505009 with water after grapefruit juice pre-treatment	100 mg			Batch L0505009 from observed *in vitro* dissolution data in simple buffers	3.55(B)

(A): Ho et al. have shown than 70% of CYP3A gut activity can be inhibited by treatment with grapefruit juice [36]. Scaling factor for gut CYP3A4 V_{max} in model is set at 0.3 to account for the reduction in CYP activity. (B): The normal default model value for fasted pH in the stomach is raised from 1.3 to 3.55, which is the calculated surface pH for acalabrutinib at bulk pH of 1.3 (C): The stomach pH in the model is raised to pH 5.54 which corresponds to the surface pH of acalabrutinib crystals when the bulk pH is at 5. This pH is that of the dosing water, assuming it controls the pH of stomach where hydrochloric acid secretion is inhibited. (D): Measured surface pH of acalabrutinib in juices.

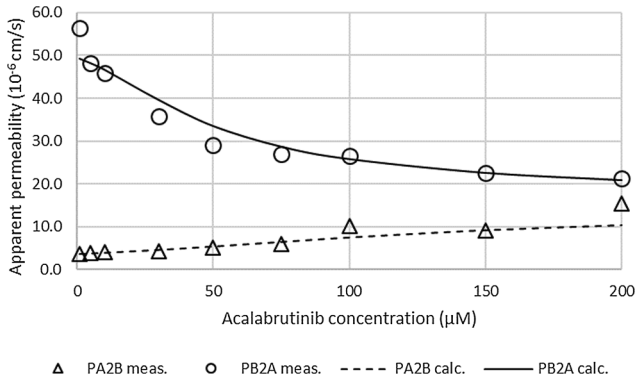

Fig. 2. Bi-directional permeability values of acalabrutinib in MDCK-MDR1 cells measured and fitted with Tachibana model.

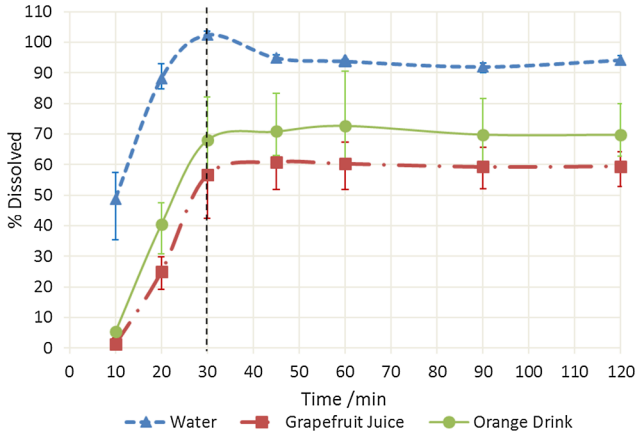

Fig. 3. Dissolution rate of 100 mg acalabrutinib capsule batch L0505009 in 60 mL SGF + 240 mL orange juice or grapefruit juice added at room temperature. Shift to FaSSIF-V2 medium at t = 30 min (dashed line). (For interpretation of the references to colour in this figure legend, the reader is referred to the web version of this article.)

emptying rate, and CYP3A4 activity. Although it is easy to measure stomach pH in fasted and fed states with technologies such as the Smartpill® [38] or Intellicap® [39], the gastric emptying rate can only be measured using systemic markers or imaging technology [40].

Alternatively, gastric-retention times can be inferred from the PK profiles of the drug itself, when clear lag times are observed in the PK profiles [8,10] or from a co-administered drug. For a largely pre-systemically metabolized drug, it is important to confirm that no metabolite appears in the blood prior to the parent drug, which could be one reason for a "lag time". For acalabrutinib, lag times observed for parent compound were also observed for the metabolite ACP-5862, indicating no absorption is taking place during the lag time (data not shown).

For drug permeability, no true marker of *in vivo* permeability exists, since for highly permeable compounds, the *in vivo* absorption rate is usually a marker of gastric-emptying. If gastric emptying is assessed separately with an appropriate marker and introduced in a mechanistic PBPK model, then permeability can be estimated from the oral plasma profiles from the PBPK model. Finally, independent determination of individual variability in CYP3A4 activity may soon be possible [41,42], however current biomarkers lack the resolution needed to determine inter-subject variability when the population is homogeneous, i.e. when there is no major induction, inhibition or genetic polymorphism that controls expression [43,44].

In conclusion, the PBPK model set-up used a top-down approach on oral and IV PK data obtained from 8 individual subjects to build a representative population for acalabrutinib. The only parameters that were fitted were the observed stomach retention times and gut CYP3A4 V_{max} due to lack of appropriate biomarkers and since they are known to vary within subjects. All other parameters were kept constant in the model.

3.5. Model verification and validation

The PBPK model was validated with five independent clinical trials ACE-HV-001, ACE-HV-004, ACE-HV-005, ACE-HV-112, ACE-HV-113 and sixteen different clinical scenarios (Table 3). These disparate data tested the ability of the model to simulate independent clinical data, obtained from different populations, formulations, doses, administration with acidic juices, or with higher stomach pH due to co-administration with proton pump inhibitors. Fig. 7 compares predicted versus measured C_{max} and AUC_{0-t}.

The agreement between measured and predicted AUC is very good throughout the clinical scenarios tested including study ACE-HV-005. For AUC predictions, the AFE and AAFE are 0.72 and 1.39 respectively. For C_{max}, the agreement is very good, except for study ACE-HV-005 where the predicted C_{max} is over-estimated. Individual PK profiles observed in study ACE-HV-005 show that 32% of the subjects of the

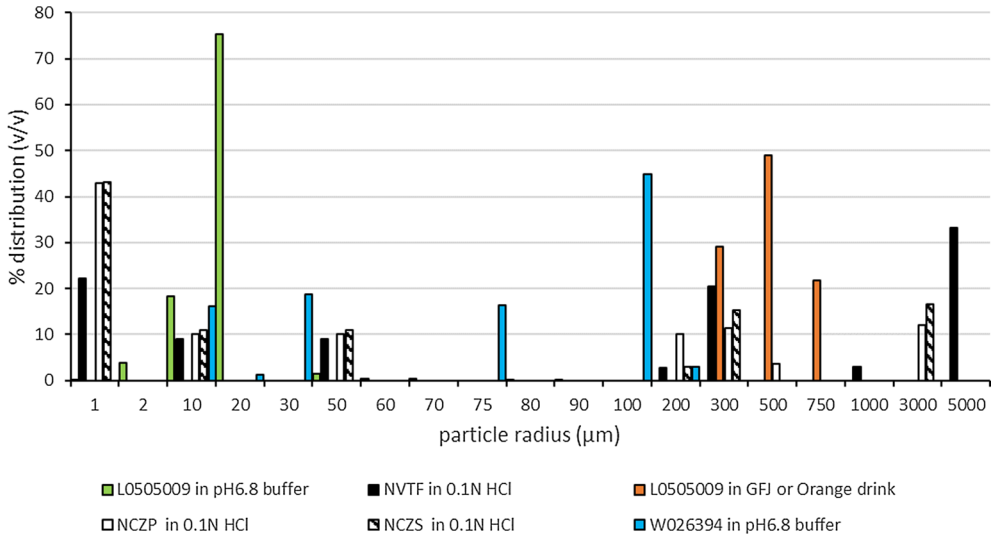

Fig. 4. P-PSD for batch L0505009 in pH6.8 buffer and orange drink or grapefruit juice, batches NCZS, NCZP, NVTF in HCl 0.1 N and W026394 in pH6.8 buffer. (For interpretation of the references to colour in this figure legend, the reader is referred to the web version of this article.)

Table 4
Individual disposition parameters by subject for cohort 1 ACE-HV-009.

Subject	S007	S008	S009	S010	S011	S012	S013	S014
BMI ($kg\,m^{-2}$)	28.6	24.5	27.9	24.6	21.4	23.0	24.0	26.8
BW (kg)	88.8	71.9	74.5	87.8	79.5	65	65.8	75.9
CL_H ($L\,h^{-1}\,kg^{-1}$)	0.296	0.580	0.365	0.486	0.692	0.694	0.494	0.380
V_c ($L\,kg^{-1}$)	0.0861	0.1825	0.0701	0.3002	0.2389	0.2447	0.1940	0.1321
k_{12} (h^{-1})	4.080	1.891	6.143	0.962	2.417	1.363	1.522	3.900
k_{21} (h^{-1})	1.955	1.911	2.651	2.249	1.633	1.645	1.882	3.700
k_{13} (h^{-1})	0.144	0.397	0.305	0.178	0.312	0.049	0.226	0.182
k_{31} (h^{-1})	0.164	0.042	0.044	0.078	0.033	0.146	0.044	0.026
V_{max} CYP3A4 ($mg\,s^{-1}$)	6.2	1.8	5.5	1.0	0.5	2.6	4.7	5.8
K_m CYP3A4 (μM)	20	20	20	20	20	20	20	20
P_{eff} ($cm\,s^{-1} \times 10^{-4}$)	5.4	5.4	5.4	5.4	5.4	5.4	5.4	5.4
V_{max} PgP ($mg\,s^{-1} \times 10^{-3}$)	4.22	4.22	4.22	4.22	4.22	4.22	4.22	4.22
K_m Pgp ($\mu g\,mL^{-1}$)	2.78	2.78	2.78	2.78	2.78	2.78	2.78	2.78

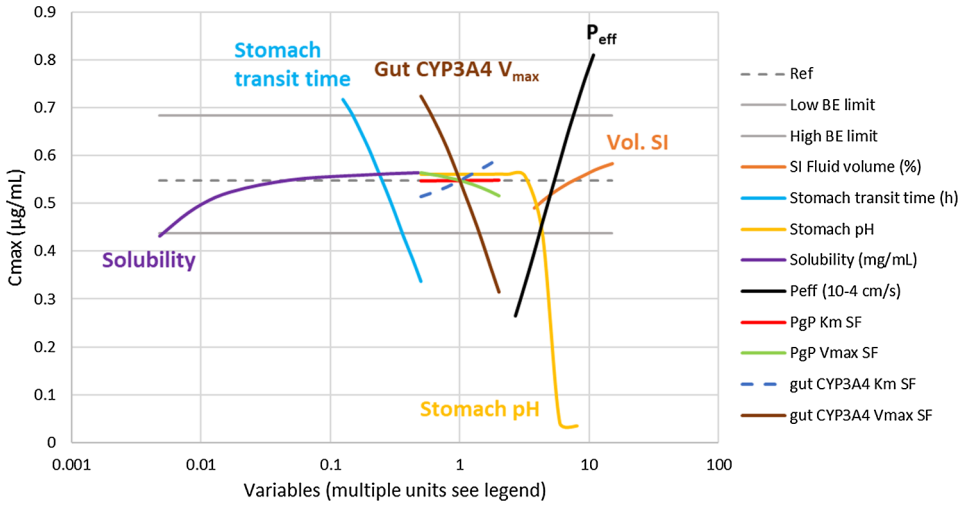

Fig. 5. Parameter sensitivity analysis probing physiological and drug dependent variables for C_{max} of 100 mg acalabrutinib capsules in subject S013.

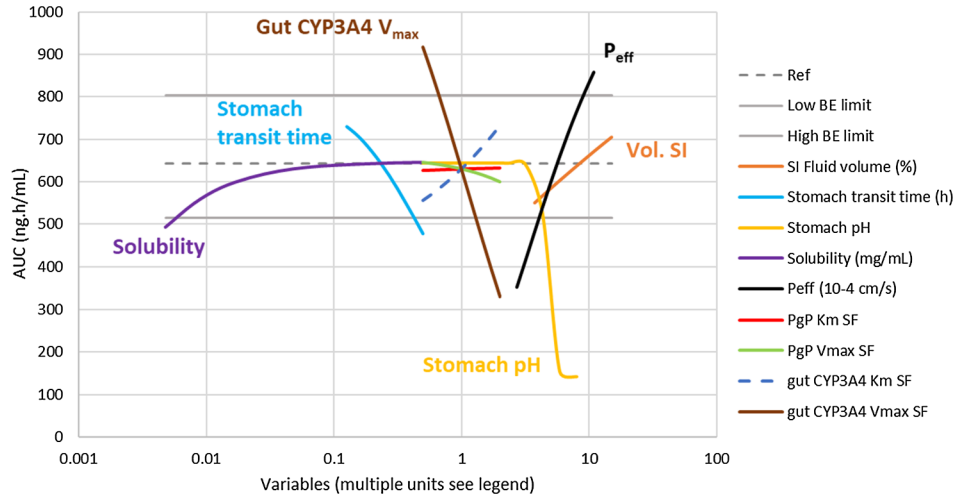

Fig. 6. Parameter sensitivity analysis probing physiological and drug dependent variables for AUC of 100 mg acalabrutinib capsules in subject S013.

100 mg arm, and 81% of the subjects of the 400 mg arm, present multiple peaks or shoulders during the drug absorption phase, which are typical of multiple phases of gastric emptying. Partial or multiple phase gastric emptying can profoundly reduce measured plasma concentrations and explain why the predictions obtained with the model (where a single-phase gastric emptying is applied) over-estimate the observed C_{max} values whilst providing for a good AUC estimate for study ACE-HV-005. Acalabrutinib capsule batch L0505009 dosed in ACE-HV-005, was also dosed in ACE-HV-009 and ACE-HV-112 where no occurrence of multiple absorption peaks was observed, ruling out any influence of the acalabrutinib capsule formulation on the occurrence of multiple peaks. In ACE-HV-005 study (thorough QTc study), a large number of dosage forms were administered, including acalabrutinib placebo capsules and moxifloxacin active or placebo tablet. In the arms reported in this work, a total of four size 1 gelatin capsules comprising active acalabrutinib or placebo and 1 moxifloxacin placebo tablet (size of 17 × 7 mm) were administered in the fasted state. When only considering the 400 mg PK data where no double peaks are

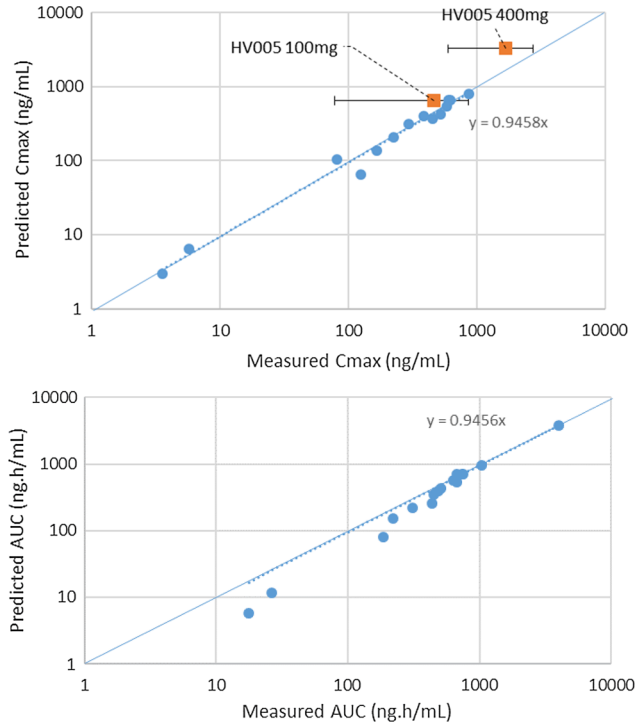

Fig. 7. Predicted and observed C_{max} (upper panel) and AUC0-t (lower panel) for the 16 different clinical scenarios of Table 3. The solid line represents unity and dashed line the correlation. Horizontal bars represent +/− 1SD. Orange symbols are C_{max} values for ACE-HV-005. (For interpretation of the references to colour in this figure legend, the reader is referred to the web version of this article.)

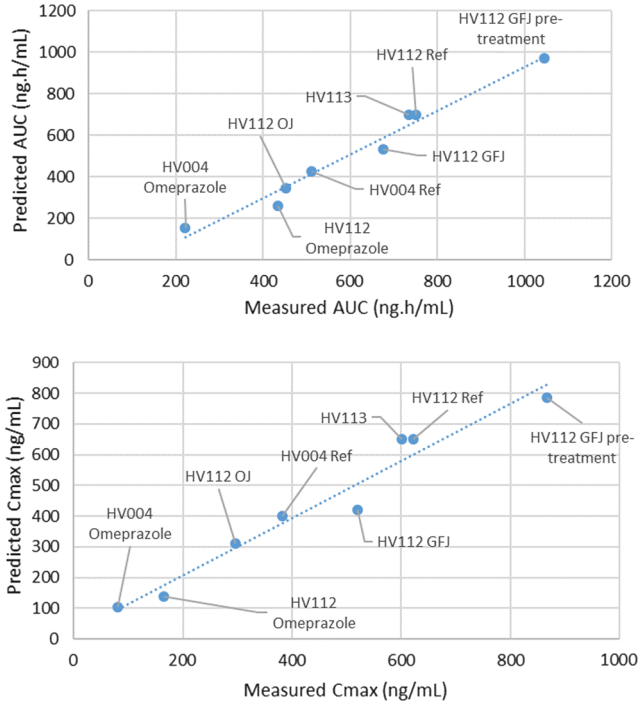

Fig. 8. Predicted vs measured AUC_{0-t} (upper panel) and C_{max} (lower panel) in ACE-HV-112, ACE-HV-113 and ACE-HV-004 for various dosing conditions.

observed (N = 8 subjects), the measured C_{max} increases to 2532 +/− 1042 ng/mL; therefore, model predictions are not significantly different from observed values.

When C_{max} data for ACE-HV-005 are omitted, the predictions for

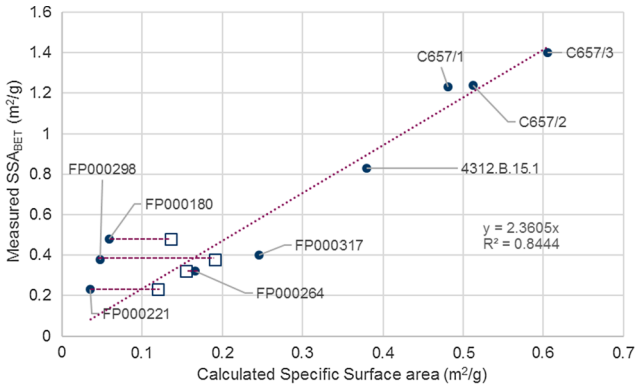

Fig. 9. Measured SSA_{BET} vs calculated SSA for selected batches. Closed symbols show calculations from laser diffraction data and open symbols from dissolution of drug product (P-PSD).

C_{max} obtained with the model are accurate. The AFE and AAFE over the 14 remaining scenarios are 0.92 and 1.17 respectively. A focus on the effect of orange drink, grapefruit juice, proton pump inhibitor (omeprazole) and formulation is provided in Fig. 8, which shows the predicted versus measured AUC_{0-t} and C_{max} for ACE-HV-112, ACE-HV-113 and ACE-HV-004.

For orange drink, it is the slower stomach dissolution that drives the incomplete absorption *in vivo*. Similar to *in vitro* dissolution, if *in vivo* drug dissolution is not complete upon stomach emptying for the juices, the overall *in vivo* absorption is reduced compared to acalabrutinib given with water. Acalabrutinib intestinal solubility is too low enable the dissolution of the drug that has not dissolved in the stomach. A sensitivity analysis was conducted on the gastric retention time for simulations of drug administration with juice. This revealed that the extent of dissolution increases with longer time spent in the stomach, which leads to drug exposure in line with what is observed when the drug is administered with water.

Acalabrutinib in grapefruit juice has similar *in vitro* dissolution to orange drink and predictions of *in vivo* absorption rate and extent are similar for both juices. As grapefruit juice results in time dependent inhibition of CYP3A, an exposure higher than that observed for orange drink is predicted when dosing the drug following grapefruit juice pre-treatment, since the fraction of drug escaping first pass gut metabolism is larger. This is well captured by the model for both C_{max} and AUC.

The impact of omeprazole and of formulation on exposure is well illustrated by comparing studies ACE-HV-112 and ACE-HV-004. In study ACE-HV-004 the dissolution of the 100 mg phase I capsule (NVTF) was slow in the QC dissolution medium resulting in large predicted P-PSD. Conversely, in study ACE-HV-112, commercial representative 100 mg capsule batch L0505009 had a rapid dissolution rate in aqueous buffers leading to a small predicted P-PSD. By just changing the P-PSD in the model and stomach pH to reflect the omeprazole pre-treatment where appropriate, the PBPK model provided for a good prediction of the impact of formulation and stomach pH on the exposure to acalabrutinib.

In conclusion, the PBPK model developed from ACE-HV-009 can predict the effect of different formulations, different stomach pH conditions, the co-administration of specific beverages and/or the administration of gut CYP3A4 inhibitors on human exposure to acalabrutinib and was considered useful for prediction of the safe space for drug substance particle size.

3.6. Model application to define drug substance PSD safe space

The particle size specification for acalabrutinib was informed by clinical batch experience and by constraints related to product content uniformity. The PBPK model was used to define the safe space for this material property. Dissolution models within PBPK models assume

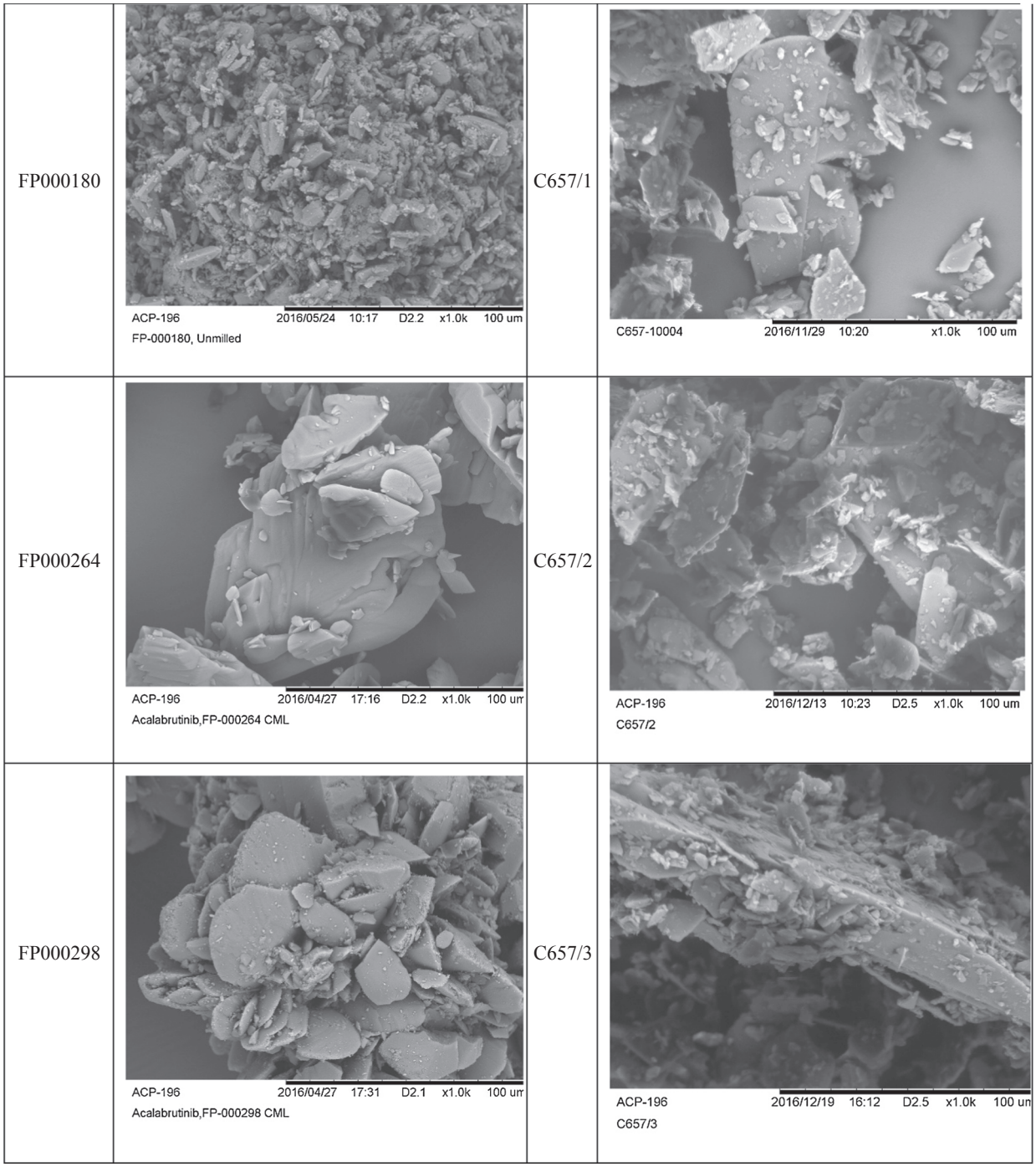

Fig. 10. SEM photographs of selected acalabrutinib drug substance batches.

spherical particle morphology for drug substances, which typically develop lower surface area than true particles, the shape of which may be very different from a sphere. Hence the ratio between the drug substance surface area available for dissolution, and the drug substance surface area calculated by PBPK models on the basis of spherical morphology, needs to be established. Evaluations were conducted to link drug substance particle size, as measured by laser diffraction (the material attribute upon which the specification is set), and drug product dissolution.

The theoretical drug substance specific surface area was calculated from the following equation, where d_i is the individual spherical particle diameter for each bin (μm) measured by laser diffraction or fitted from drug product dissolution data (P-PSD), f_i is the mass or volume fraction in each bin and, ρ_S is the true crystal density in ($g\,cm^{-3}$).

$$SSA_{calc} = \frac{1}{\rho_S} \times \sum_{1}^{n} f_i \times \frac{6}{d_i}$$

The measured versus calculated specific surface area for selected acalabrutinib drug substance batches is presented in Fig. 9, where there is an approximately 2.5-fold ratio between true surface area presented by acalabrutinib batches, and the surface area calculated on the basis of spherical particle morphology using laser diffraction data or P-PSD.

The ratio of approximately 2.5 can be explained by the non-spherical shape of the primary acalabrutinib particles, which are able to develop a larger surface area than an equivalent diameter sphere. This ratio is well preserved for the various drug substance batches

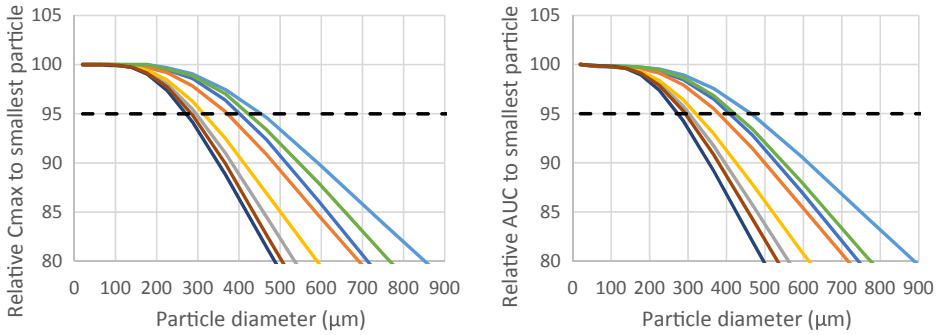

Fig. 11. C_{max} (left) and AUC (right) for each subject of ACE-HV-009 vs particle diameter, relative to values observed for a 20 µm diameter reference. Dotted line is a 95% exposure threshold relative to the reference.

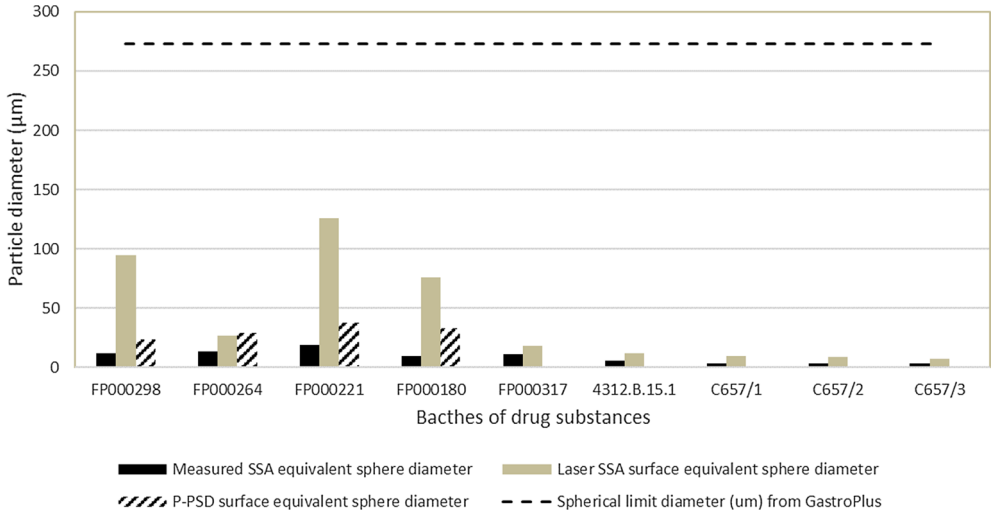

Fig. 12. Limit sphere diameter (horizontal dashed line) vs batch equivalent diameters.

manufactured during development, except for batches FP000180, FP000298 or FP000221, for which laser diffraction under-estimates even more the measured specific surface area. These batches show higher levels of aggregation of primary particles compared to the others (Fig. 10). For drug products, manufactured with drug substance batches that show particle aggregation, the prediction of surface area from dissolution derived P-PSD brings these batches closer to the overall correlation.

Since parameter sensitivity analysis in the PBPK model is conducted with only one bin for particle size, the calculation of a "surface-equivalent" diameter is needed for each batch, to be able to compare the proposed acceptable limit with real batch data. The following equation is used with all parameters described previously.

$$d_{eq} = \frac{1}{\rho_S} \times \frac{6}{SSA}$$

A sensitivity analysis was undertaken with each subject of study ACE-HV-009, to evaluate the impact of the drug substance particle size on exposure using spherical particle morphology and only one bin. Simulations were run under normal stomach pH conditions (Fig. 11).

The PSA results shown for C_{max} and AUC in Fig. 11, indicate that a spherical particle diameter up to 270 µm would lead to exposure differences of less than 5% for both C_{max} and AUC, as compared to a 20 µm diameter size reference. This limit size of 270 µm is 2 to 5 times above the observed equivalent diameters for batches of acalabrutinib, whether using measured drug substance surface area, laser diffraction or dissolution data calculated surface area to derive the particle size (Fig. 12), and illustrate the safe space for drug substance particle size.

3.7. Decision tree for dissolution data integration

Currently, several methods are available to integrate dissolution data of immediate release dosage form into a PBPK model. The approach outlined in this paper can be schematically presented in the following strategy (Fig. 13).

For immediate release products, determination of dissolution in discriminant conditions is needed to establish the link between product dissolution and drug substance particle size. This link is important to ascertain, since the surface area developed by drug substance batches may be significantly higher than calculated by PBPK models on the basis of laser diffraction data using spherical particle morphology. P-PSD batch data should be compared with particle size data of the drug substance used for product manufacture, since the manufacturing process and excipients may lead to changes in the drug substance surface available for dissolution. For acalabrutinib drug product a 2-fold underprediction of *in vitro* dissolution rate was shown using drug substance particle size distribution as an input to predict dissolution.

Adaptations to current PBPK models are required in some situations. These mainly include the use of surface pH in the compartments of the gastro-intestinal tract where the drug is reactive. For a weak base such as acalabrutinib where the maximum basic pKa is less than 6, only the stomach is concerned with pH adjustment. For stronger bases, if the basic pKa is higher than 6, pH adaptations in more or all the GI-tract segments may be needed.

The approach illustrated in this paper and previously for a weak acid [8], show that the derivation and use of a P-PSD for each product batch as an input to PBPK modelling platforms is clinically relevant, even when it is derived from QC method dissolution experiments, and

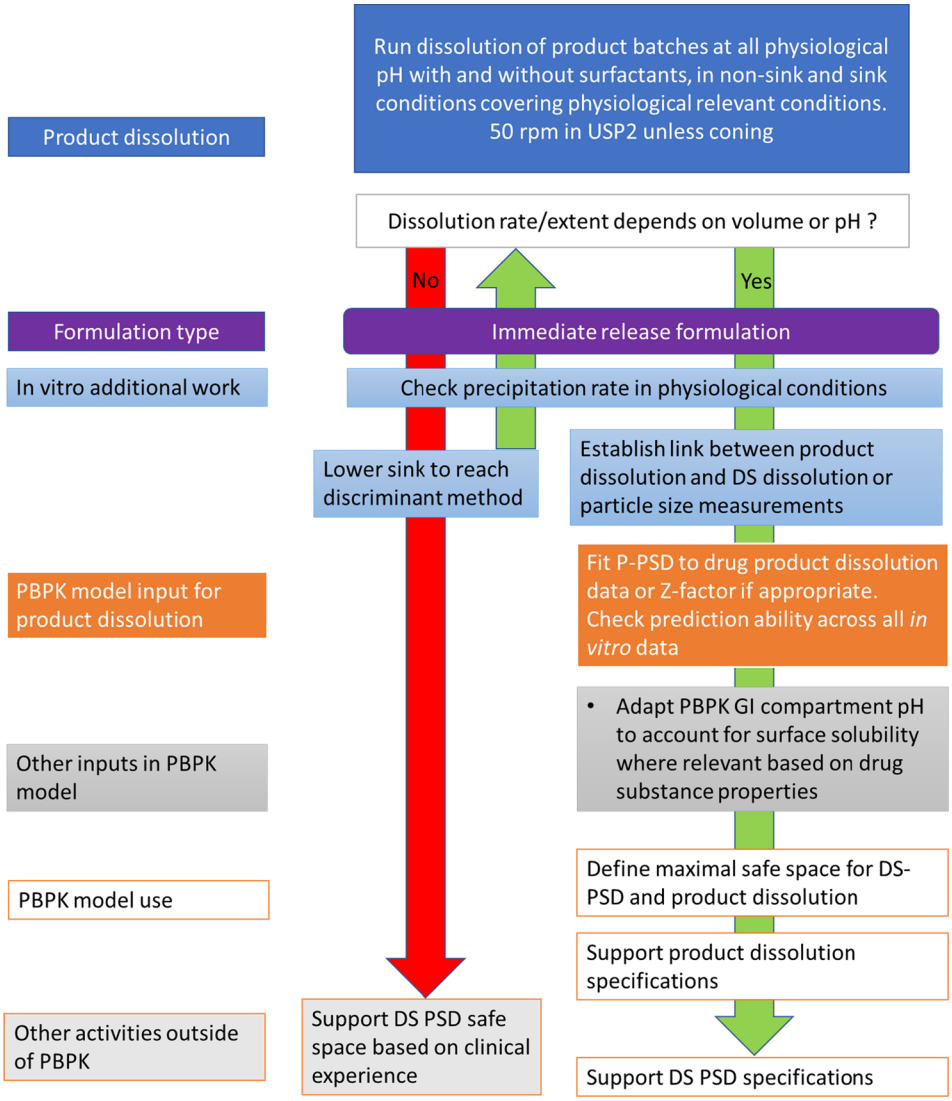

Fig. 13. Integration of drug product dissolution data in PBPK.

can be used to predict important clinical study outcomes, such as the impact of formulation changes, different gastro-intestinal pH conditions, or the administration of different fluids with the drug [11]

4. Conclusions and perspectives

This work demonstrates the utility of the Product Particle Size Distribution (P-PSD) extracted from *in vitro* data as an input to a PBPK model. In simple media, using the right surface pH, they provide a meaningful tool to bridge between *in vitro* and *in vivo* drug product dissolution. For acalabrutinib, a weak diprotic base, the consideration of surface pH to explain *in vitro* and *in vivo* dissolution is needed, but GastroPlus v9.0 or Simcyp v15 cannot currently calculate this value. Manual alteration of the stomach pH can help circumvent this issue for acalabrutinib, but the integration in PBPK models of drug related surface pH calculations, in all the segments of the GI-tract based on the drug solubility, ionization constants, and molecular weight, would represent an improvement to calculate the *in vivo* dissolution of reactive drugs without having to manually change the physiological pH conditions. Despite these limitations, PBPK models appear to be good candidates to predict the outcome of Acid Reducing Agents (ARAs) studies which are of importance for weak bases or to understand the impact of natural pH variations in the stomach [11]. Because the P-PSD is based on a mechanistic understanding of *in vitro* dissolution, the prediction of clinical ARA study outcomes can be done by simply changing the stomach pH. In addition, since the P-PSD is batch specific, it can also be used to capture the effect of changes in the formulation on the human PK.

Verification of the dissolution performance of drug product in simple and complex media is encouraged, including beverages used in the clinic or in the day to day administration of the drugs, since surface reactions during dissolution in certain beverages can be slower than in water. The clinical observations reported in the literature where drug exposure is reduced with fruit juices are qualitatively explained in most cases by invoking transporter interactions with juice components. Some of these reported cases concern weakly basic drug substances with low intestinal solubility, that may react with juice acid components in the stomach. For these drugs, dissolution testing in juice may offer alternative explanation to the impact of juice on the drug pharmacokinetics using the approach illustrated in this paper.

Currently, mechanistic dissolution equations present in most PBPK models, excepted for GCoas v1.1 (Process Systems Enterprise Ltd.), do not consider the impact of fluid components on dissolution rate. In addition, since sodium bicarbonate, the biologically relevant buffer, is different from the buffers used *in vitro*, a more accurate calculation of *in vivo* dissolution would benefit from integrating these parameters.

Finally, the understanding and modelling of individual pharmacokinetic profiles would benefit from the development and use of adapted biomarkers. Fitting of average PK profiles is sometimes confounding,

especially for a rapidly cleared product or when the drug shows variable lag times in its absorption phase. Simple biomarkers for stomach pH and transit time should be used to support the mechanistic understanding of individual PK profiles in addition to intra-venous microdosing information when required.

Appendix A. Supplementary material

Supplementary data to this article can be found online at https://doi.org/10.1016/j.ejpb.2019.07.011.

References

[1] T. Mirza, et al., Use of in vitro-in vivo correlation to predict the pharmacokinetics of several products containing a BCS class 1 drug in extended release matrices, Pharm. Res. 30 (1) (2013) 179–190.
[2] S. Suarez-Sharp, et al., Regulatory experience with in vivo in vitro correlations (IVIVC) in new drug applications, AAPS J. 18 (6) (2016) 1379–1390.
[3] A. Abend, et al., Dissolution and translational modeling strategies enabling patient-centric drug product development: the M-CERSI workshop summary report, AAPS J. 20 (3) (2018).
[4] V.R. Uppoor, Regulatory perspectives on in vitro (dissolution)/in vivo (bioavailability) correlations, J. Control. Rel.: Offic. J. Control. Rel. Soc. 72 (1–3) (2001) 127–132.
[5] M.A. Nguyen, et al., A survey on IVIVC/IVIVR development in the pharmaceutical industry - past experience and current perspectives, Euro. J. Pharm. Sci.: Offic. J. Euro. Feder. Pharm. Sci. 102 (2017) 1–13.
[6] A. Okumu, M. DiMaso, R. Lobenberg, Dynamic dissolution testing to establish in vitro/in vivo correlations for montelukast sodium, a poorly soluble drug, Pharm. Res. 25 (12) (2008) 2778–2785.
[7] P. Dickinson, et al., Clinical relevance of dissolution testing in quality by design, AAPS J. 10 (2) (2008) 380–390.
[8] X.J.H. Pepin, et al., Justification of drug product dissolution rate and drug substance particle size specifications based on absorption PBPK modeling for lesinurad immediate release tablets, Mol. Pharm. 13 (9) (2016) 3256–3269.
[9] Dissolution and Translational Modeling Strategies Enabling Patient-Centric Product Development. in M-CERSI. 2017. Baltimore.
[10] C.J. Andreas, et al., Mechanistic investigation of the negative food effect of modified release zolpidem, Eur. J. Pharm. Sci. 102 (2017) 284–298.
[11] R. Cristofoletti, N. Patel, J.B. Dressman, Assessment of bioequivalence of weak base formulations under various dosing conditions using physiologically based pharmacokinetic simulations in virtual populations. Case examples: ketoconazole and posaconazole, J. Pharm. Sci. 106 (2) (2017) 560–569.
[12] D. Riethorst, et al., Characterization of human duodenal fluids in fasted and fed state conditions, J. Pharm. Sci. 105 (2) (2016) 673–681.
[13] G.L. Shih, et al., Influence of age and gender on gastric acid secretion as estimated by integrated acidity in patients referred for 24-hour ambulatory pH monitoring, Am. J. Gastroenterol. 98 (8) (2003) 1713–1718.
[14] W.K. Fackler, M.F. Vaezi, J.E. Richter, Ambulatory gastric pH monitoring: proper probe placement and normal values, Aliment. Pharmacol. Ther. 15 (8) (2001) 1155–1162.
[15] E.F. Verdú, et al., Effect of Helicobacter pylori status on intragastric pH during treatment with omeprazole, Gut 36 (4) (1995) 539–543.
[16] P. Mojaverian, et al., Effects of gender, posture, and age on gastric residence time of an indigestible solid: pharmaceutical considerations, Pharm. Res. 5 (10) (1988) 639–644.
[17] M. Morihara, et al., Assessment of gastric acidity of Japanese subjects over the Last 15 Years, Biol. Pharm. Bull. 24 (3) (2001) 313–315.
[18] T.S. Papavramidis, et al., Pre- and postoperative esophageal and gastric pH levels in morbidly obese patients undergoing vertical gastroplasty, Obes. Surg. 14 (2) (2004) 271–274.
[19] D. de Wit, et al., Effect of gastrointestinal resection on sunitinib exposure in patients with GIST, BMC Cancer 14 (2014) 575.
[20] N.R. Budha, et al., Drug absorption interactions between oral targeted anticancer agents and PPIs: is pH-dependent solubility the achilles heel of targeted therapy? Clin. Pharmacol. Ther. 92 (2) (2012) 203–213.
[21] L. Zhang, et al., pH-dependent drug-drug interactions for weak base drugs: potential implications for new drug development, Clin. Pharmacol. Ther. 96 (2) (2014) 266–277.
[22] R.W.F. van Leeuwen, et al., Influence of the acidic beverage cola on the absorption of erlotinib in patients with non-small-cell lung cancer, J. Clin. Oncol. 34 (12) (2016) 1309–1314.
[23] P. Pohl, S.M. Saparov, Y.N. Antonenko, The size of the unstirred layer as a function of the solute diffusion coefficient, Biophys. J. 75 (3) (1998) 1403–1409.
[24] W.I. Higuchi, E.L. Parrott, D.E. Wurster, T. Higuchi, Investigation of drug release from solids II. Theoretical and experimental study of influences of bases and buffers on rates of dissolution of acidic solids, J. Am. Pharm. Assoc. 67 (5) (1958) 376–383.
[25] E. Jantratid, et al., Dissolution media simulating conditions in the proximal human gastrointestinal tract: an update, Pharm. Res. 25 (7) (2008) 1663–1676.
[26] E. Galia, et al., Evaluation of various dissolution media for predicting in vivo performance of class I and II drugs, Pharm. Res. 15 (5) (1998) 698–705.
[27] T. Tachibana, et al., Model analysis of the concentration-dependent permeability of P-gp substrates, Pharm. Res. 27 (3) (2010) 442–446.
[28] M. Troutman, D. Thakker, Novel experimental parameters to quantify the modulation of absorptive and secretory transport of compounds by P-glycoprotein in cell culture models of intestinal epithelium, Pharm. Res. 20 (8) (2003) 1210–1224.
[29] H. Lennernäs, Intestinal permeability and its relevance for absorption and elimination, Xenobiotica 37 (10–11) (2007) 1015–1051.
[30] A.T.M. Serajuddin, C.I. Jarowski, Effect of diffusion layer pH and solubility on the dissolution rate of pharmaceutical bases and their hydrochloride salts I: phenazopyridine, J. Pharm. Sci. 74 (2) (1985) 142–147.
[31] R. Takano, et al., Oral absorption of poorly water-soluble drugs: computer simulation of fraction absorbed in humans from a miniscale dissolution test, Pharm Res 23 (6) (2006) 1144–1156.
[32] T. Barf, et al., Acalabrutinib (ACP-196): a covalent bruton tyrosine kinase inhibitor with a differentiated selectivity and in vivo potency profile, J. Pharmacol. Exp. Therap. 363 (2) (2017) 240–252.
[33] CDER, F. Highlights of Prescribing Information. CALQUENCE® (acalabrutinib) capsules, for oral use Initial U.S. Approval: 2017 2017 [cited 2017 12/12/2017]; Available from: https://www.accessdata.fda.gov/drugsatfda_docs/label/2017/210259s000lbl.pdf.
[34] C. Schiller, et al., Intestinal fluid volumes and transit of dosage forms as assessed by magnetic resonance imaging, Aliment Pharmacol. Ther. 22 (10) (2005) 971–979.
[35] K.S. Lown, et al., Interpatient heterogeneity in expression of CYP3A4 and CYP3A5 in small bowel. Lack of prediction by the erythromycin breath test, Drug Metab. Disposit.: Biol. Fate Chem. 22 (6) (1994) 947–955.
[36] P.C. Ho, D.J. Saville, S. Wanwimolruk, Inhibition of human CYP3A4 activity by grapefruit flavonoids, furanocoumarins and related compounds, J. Pharm. Pharm. Sci. 4 (3) (2001) 217–227.
[37] A.S. Darwich, et al., IMI - Oral biopharmaceutics tools project - evaluation of bottom-up PBPK prediction success part 3: identifying gaps in system parameters by analysing In silico performance across different compound classes, Eur. J. Pharm. Sci. 96 (2017) 626–642.
[38] M. Koziolek, et al., Intragastric pH and pressure profiles after intake of the high-caloric, high-fat meal as used for food effect studies, J. Contr. Rel. 220 (Pt A) (2015) 71–78.
[39] E. Sjogren, et al., In vivo methods for drug absorption - comparative physiologies, model selection, correlations with in vitro methods (IVIVC), and applications for formulation/API/excipient characterization including food effects, Eur. J. Pharm. Sci. 57 (2014) 99–151.
[40] S. Bluemel, et al., On the validity of the (13) C-acetate breath test for comparing gastric emptying of different liquid test meals: a validation study using magnetic resonance imaging, Neurogastroenterol. Motil.: Offic. J. Europ. Gastrointest. Motil. Soc. 27 (10) (2015) 1487–1494.
[41] U. Diczfalusy, et al., 4β-hydroxycholesterol, an endogenous marker of CYP3A4/5 activity in humans: 4β-hydroxycholesterol, an endogenous marker of CYP3A4/5 activity, Br. J. Clin. Pharmacol. 71 (2) (2011) 183–189.
[42] D. Wang, W. Sadee, The making of a CYP3A biomarker panel for guiding drug therapy, J. Personal. Med. 2 (4) (2012) 175–191.
[43] T.A. Leil, et al., Evaluation of 4β-hydroxycholesterol as a clinical biomarker of CYP3A4 drug interactions using a bayesian mechanism-based pharmacometric model, CPT: Pharmacometr. Syst. Pharmacol. (2014) 3.
[44] S.J. Woolsey, et al., Relationships between endogenous plasma biomarkers of constitutive cytochrome P450 3A activity and single-time-point oral midazolam microdose phenotype in healthy subjects, Basic Clin. Pharmacol. Toxicol. 118 (4) (2016) 284–291.
[45] X.J.H. Pepin, N.J. Sanderson, A. Blanazs, S. Grover, T.G. Ingallinera, J.C. Mann, Bridging in vitro dissolution and in vivo exposure for acalabrutinib. Part I. Mechanistic modelling of drug product dissolution to derive a P-PSD for PBPK model input, Eur. J. Pharmaceut. Biopharmaceut. (2019), https://doi.org/10.1016/j.ejpb.2019.07.014.